

Boosting the performance of crossed ZnO microwire UV photodetector by mechanical contact homo-interface barrier

Yinzhe Liu(刘寅哲), Kewei Liu(刘可为), Jialin Yang(杨佳霖), Zhen Cheng(程祯), Dongyang Han(韩冬阳), Qiu Ai(艾秋), Xing Chen(陈星), Yongxue Zhu(朱勇学), Binghui Li(李炳辉), Lei Liu(刘雷), and Dezhen Shen(申德振)

Citation: Chin. Phys. B, 2022, 31 (**10**): 106101. DOI: 10.1088/1674-1056/ac80b0
Journal homepage: http://cpb.iphy.ac.cn; http://iopscience.iop.org/cpb

What follows is a list of articles you may be interested in

Migration of weakly bonded oxygen atoms in a-IGZO thin films and the positive shift of threshold voltage in TFTs

Chen Wang(王琛), Wenmo Lu(路文墨), Fengnan Li(李奉南), Qiaomei Luo(罗巧梅), and Fei Ma(马飞)†
Chin. Phys. B, 2022, 31 (**9**): 096101. DOI: 10.1088/1674-1056/ac560f

Combined effects of cycling endurance and total ionizing dose on floating gate memory cells

Si-De Song(宋思德), Guo-Zhu Liu(刘国柱), Qi He(贺琪), Xiang Gu(顾祥), Gen-Shen Hong(洪根深), and Jian-Wei Wu(吴建伟)
Chin. Phys. B, 2022, 31 (**5**): 056107. DOI: 10.1088/1674-1056/ac3d80

Evolution of defects and deformation mechanisms in different tensile directions of solidified lamellar Ti-Al alloy

Yutao Liu(刘玉涛), Tinghong Gao(高廷红), Yue Gao(高越), Lianxin Li(李连欣), Min Tan(谭敏), Quan Xie(谢泉), Qian Chen(陈茜), Zean Tian(田泽安), Yongchao Liang(梁永超), and Bei Wang(王蓓)
Chin. Phys. B, 2022, 31 (**4**): 046105. DOI: 10.1088/1674-1056/ac1f0b

Effect of heavy ion irradiation on the interface traps of AlGaN/GaN high electron mobility transistors

Zheng-Zhao Lin(林正兆), Ling Lü(吕玲), Xue-Feng Zheng(郑雪峰), Yan-Rong Cao(曹艳荣), Pei-Pei Hu(胡培培), Xin Fang(房鑫), and Xiao-Hua Ma(马晓华)
Chin. Phys. B, 2022, 31 (**3**): 036103. DOI: 10.1088/1674-1056/ac11e4

Nanoscale structural investigation of $Zn_{1-x}Mg_xO$ alloy films on polar and nonpolar ZnO substrates with different Mg contents

Xin Liang(梁信), Hua Zhou(周华), Hui-Qiong Wang(王惠琼), Lihua Zhang(张丽华), Kim Kisslinger, and Junyong Kang(康俊勇)
Chin. Phys. B, 2021, 30 (**9**): 096107. DOI: 10.1088/1674-1056/ac11e1

RAPID COMMUNICATION

Boosting the performance of crossed ZnO microwire UV photodetector by mechanical contact homo-interface barrier

Yinzhe Liu(刘寅哲)[1,2], Kewei Liu(刘可为)[1,2,†], Jialin Yang(杨佳霖)[1,2], Zhen Cheng(程祯)[1,2], Dongyang Han(韩冬阳)[1,2], Qiu Ai(艾秋)[1,2], Xing Chen(陈星)[1,2], Yongxue Zhu(朱勇学)[1,2], Binghui Li(李炳辉)[1,2], Lei Liu(刘雷)[1,2], and Dezhen Shen(申德振)[1,2,‡]

[1] *State Key Laboratory of Luminescence and Applications, Changchun Institute of Optics, Fine Mechanics and Physics, Chinese Academy of Sciences, Changchun* 130033, *China*

[2] *Center of Materials Science and Optoelectronics Engineering, University of Chinese Academy of Sciences, Beijing* 100049, *China*

(Received 12 June 2022; revised manuscript received 11 July 2022; accepted manuscript online 13 July 2022)

One-dimensional (1D) micro/nanowires of wide band gap semiconductors have become one of the most promising blocks of high-performance photodetectors. However, in the axial direction of micro/nanowires, the carriers can transport freely driven by an external electric field, which usually produces large dark current and low detectivity. Here, an UV photodetector built from three cross-intersecting ZnO microwires with double homo-interfaces is demonstrated by the chemical vapor deposition and physical transfer techniques. Compared with the reference device without interface, the dark current of this ZnO double-interface photodetector is significantly reduced by nearly 5 orders of magnitude, while the responsivity decreases slightly, thereby greatly improving the normalized photocurrent-to-dark current ratio. In addition, ZnO double-interface photodetector exhibits a much faster response speed ($\sim$ 0.65 s) than the no-interface device ($\sim$ 95 s). The improved performance is attributed to the potential barriers at the microwire–microwire homo-interfaces, which can regulate the carrier transport. Our findings in this work provide a promising approach for the design and development of high-performance photodetectors.

Keywords: ZnO microwire, interface, potential barrier, dark current, photocurrent-to-dark current ratio

PACS: 61.46.Km, 61.72.uj, 61.80.Ba, 62.23.Hj **DOI:** 10.1088/1674-1056/ac80b0

1. Introduction

Ultraviolet (UV) photodetectors based on wide band gap semiconductors (GaN, ZnO, Ga_2O_3, etc.) have attracted considerable attention in recent years due to their great potential in both military and civilian applications.[1–9] Owing to the high crystalline quality, large surface-to-volume ratio and effective charges separation, one-dimensional (1D) micro/nanowires have become one of the most promising building blocks for high-performance photodetectors.[10–18] Up to now, numerous UV photodetectors have been realized based on individual 1D micro/nanowire of different wide band gap semiconductors, such as ZnO, SnO_2, GaN and so on.[19–28] Most of the reported devices are built on a simple metal–semiconductor–metal (MSM) structure with a single 1D micro/nanowire as the active light-collecting region. It has been demonstrated that individual 1D micro/nanowire photodetectors usually have ultrahigh photocurrent gains (10^5–10^9).[19–28] And these high gains are generally considered to be related to the trapping effect and the enhanced electron–hole separation due to the energy band bending induced by surface states in the radial direction of micro/nanowires.[25,26] However, in the axial direction of micro/nanowires, the carriers can transport freely under the drive of an external electric field, which often produce large dark current and low detectivity.[24,29–32] One of the most common approaches to resolve the above problem is constructing axial heterojunctions, such as pn junction,[33,34] quantum well,[35] superlattice[36–38] and inserting a barrier layer,[39–41] which could effectively modulate the carriers separation and transport in the axial direction. However, it remains a challenge to obtain high-quality and abrupt heterojunction interface along the growth axis.[42–44]

In this work, taking ZnO microwire as an example, we demonstrate a significant performance enhancement of ZnO microwire UV photodetector by introducing mechanical contact homo-interfaces. 1D ZnO micro/nanowires are excellent candidates for UV photodetectors due to their wide direct band gap, easy fabrication, high radiation hardness and high saturation electron drift velocity.[23,25,26,45] The UV photodetector is built from three cross-intersecting ZnO microwires with double microwire–microwire homo-interfaces. Compared with the no-interface reference device, the double-interface photodetector not only exhibits lower dark current and higher detectivity, but also has a faster response speed. The systematic comparative studies reveal that the potential barriers formed at the intersections of ZnO microwires could modulate the carrier transport along the axial direction of the microwires, thereby significantly reducing the dark current and increas-

[†]Corresponding author. E-mail: liukw@ciomp.ac.cn
[‡]Corresponding author. E-mail: shendz@ciomp.ac.cn

© 2022 Chinese Physical Society and IOP Publishing Ltd

ing the normalized photocurrent-to-dark current ratio (NPDR). Moreover, the quick change of barrier heights induced by turning on or off the UV light could promote the response speed of the device.

2. Experimental details

2.1. Preparation of ZnO microwires

ZnO microwires were synthesized via a simple one-step chemical vapor deposition (CVD) method,[46,47] using a mixture of ZnO powders and graphite powders (1:1 in weight ratio) as the reactant source material. The alumina boat containing the mixed powders was placed in the center of the furnace. After that, the temperature of the boat was increased to 1030 °C, and maintained at this temperature for 60 min to fabricate ZnO microwires. Ar (4N) and O_2 (5N) were used as the carrier gas and oxygen source at flow rates of 100 sccm and 10 sccm, respectively. After the growth, the furnace was naturally cooled to room temperature and continuously vented with oxygen and argon.

2.2. Characterizations of the materials and devices

The morphology of the samples was characterized by scanning electron microscope (SEM, Hitachi S-4800) and helium ion microscope (HIM, Zeiss Orion NanoFab). And the crystalline structure was tested by x-ray diffraction (XRD, Bruker D8GADDS). Photoluminescence (PL) measurement was carried out with a laser Raman spectrometer (VV-LABRAM). The current–voltage (I–V) and time-dependent current (I–t) characteristics of the device were measured using a semiconductor device analyzer (Agilent B1500A). The response spectra were measured by using a 200 W UV-enhanced Xe lamp and a monochromator.

3. Results and discussion

Schematic fabrication process of the crossed ZnO microwire photodetectors is shown in Fig. 1. Highly crystallized ZnO microwires were formed at the downstream end of the alumina boat. A sharp tweezer was used to pick up ZnO microwires one by one from the ceramic boat and place them on a glass substrate to build a cross-stacked architecture. After that, indium ball electrodes were drop cast manually on both ends of each microwire and heated on a hotplate at 200 °C to improve the contact property. In this cross-stacked architecture, three ZnO microwires have the similar diameter and properties.

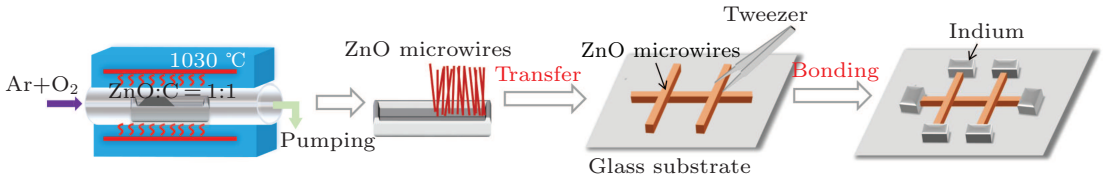


Fig. 1. Schematic fabrication process of the crossed ZnO microwire photodetectors.

Figure 2(a) shows the SEM image of single ZnO microwire. It can be seen that the morphology of ZnO microwires is a quadrangular prism with a diameter of ∼ 10 μm. Moreover, the surface of the microwires is very smooth and flat. Figure 2(b) presents the HIM image of the crossed microwire architecture. Obviously, the microwires are in close physical contact with each other. The XRD spectrum of the ZnO microwires dispersed on a glass substrate is shown in Fig. 2(c). The sharp diffraction peaks at 32°, 34.7°, 36.5° and 47.8° can be assigned to (100), (002), (101) and (102) planes of wurtzite ZnO. All the peaks are matching with the ZnO hexagonal phase of JCPDF No. 36-1451. Figure 2(d) presents the PL spectrum of ZnO microwires at room temperature. A strong UV emission is clearly observed at ∼ 380 nm, which can be attributed to the near-band edge (NBE) emission of ZnO.[29,32,47,48] Besides, a shoulder signal is also observed near the NBE emission, which can be originated from the phonon replica of free exciton luminescence.[49] In addition, a weak and broad visible emission band centered at ∼ 520 nm is generally considered to come from the oxygen vacancy defect in ZnO.[29,47] The PL spectrum suggests that the ZnO microwires fabricated in this work have a few oxygen vacancy defects.

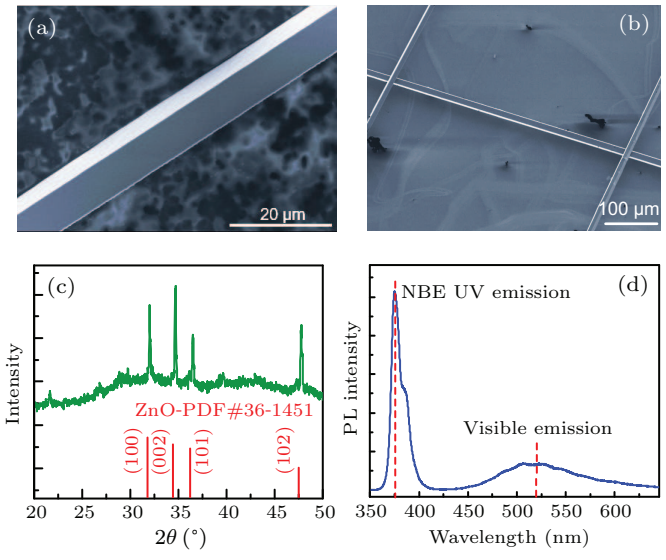


Fig. 2. (a) SEM image of single ZnO microwire. (b) HIM image of the crossed microwire architecture. (c) XRD and (d) PL results of ZnO microwires.

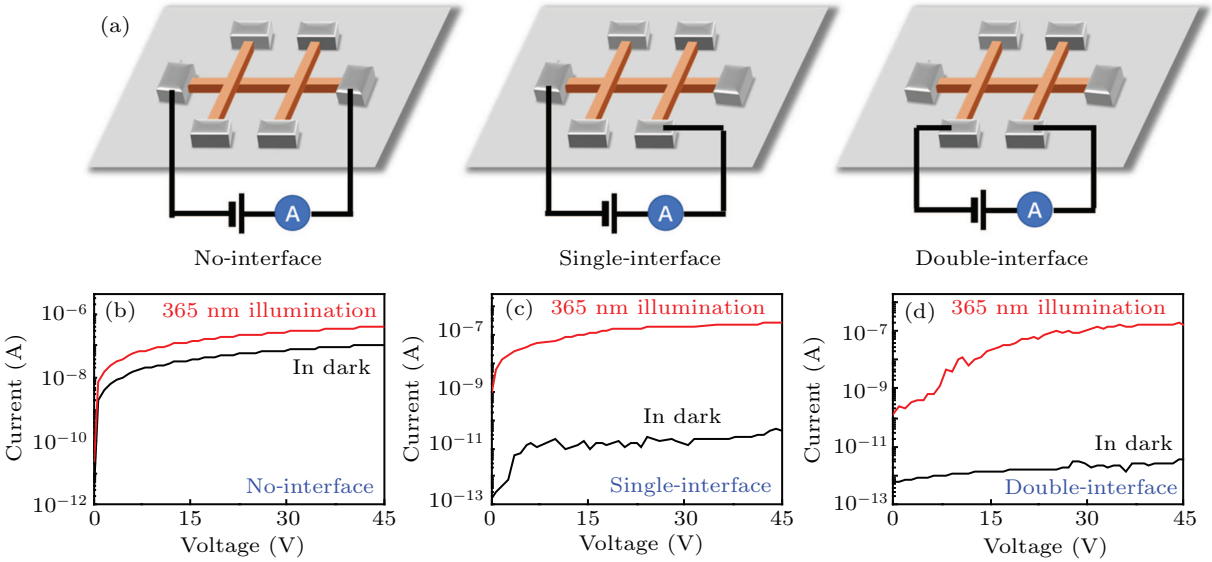


Fig. 3. (a) Schematic diagram of no-interface, single-interface, and double-interface ZnO microwire photodetectors. The *I*–*V* characteristics of (b) no-interface, (c) single-interface, and (d) double-interface devices in the dark (black line) and under 365 nm illumination at a power density of ~ 0.8 mW/cm^2 (red line).

To investigate the interface effect on the photodetection performance, in addition to the ZnO double-interface UV photodetector, the reference devices without interface and with single interface were also prepared as shown in Fig. 3(a). To avoid the influence of device length, the lengths of the three devices are similar ($\sim$ 1 cm). In addition, because adsorbed gas molecules, such as O_2 and H_2O, have a great impact on the photoelectric performance of microwires,[50] the three devices are tested in the air environment with same humidity. Figures 3(b), 3(c) and 3(d) show the *I*–*V* curves in the dark and under the 365 nm illumination (~ 0.8 mW/cm^2) of the no-interface, single-interface and double-interface devices, respectively. In Fig. 3(b), a relatively large dark current of $\sim 1.11 \times 10^{-7}$ A can be observed at 45 V bias for the reference device without interface due to the large number of background carriers in the ZnO microwire. Under the UV illumination, the current of the device increases to about 4.06×10^{-7} A at 45 V. With the introduction of the microwire–microwire interface, the dark current of ZnO UV photodetector with single and double interfaces has been significantly reduced as shown in Figs. 3(c) and 3(d), respectively. Notably, the double-interface device exhibits an ultra-low dark current of $\sim 3.52 \times 10^{-12}$ A at 45 V bias, which is nearly 5 orders of magnitude lower than that of no-interface reference device.

Figure 4 shows the spectral response of ZnO microwire photodetectors with and without interface at 45 V bias in the wavelength range from 340 nm to 700 nm. All three devices exhibit a broad response peak centered at $\sim$ 370 nm and a sharp -3 dB cutoff wavelength of $\sim$ 380 nm, which precisely corresponds to the band gap of ZnO ($\sim$ 3.37 eV at room temperature). The peak responsivities of no-interface, single-interface, and double-interface ZnO photodetectors are 120 mA/W, 90 mA/W and 80 mA/W, respectively. In addition, the UV/visible rejection ratio ($R_{\text{peak}}/R_{550\text{ nm}}$) of all three devices can reach nearly 10^3.

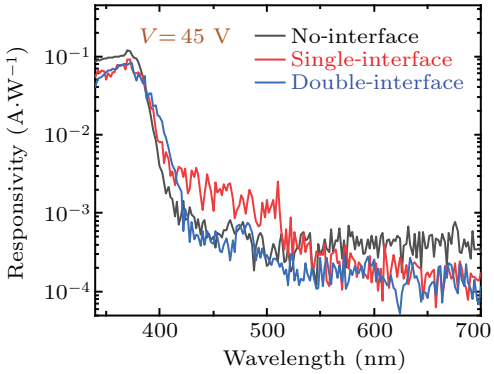


Fig. 4. The photoresponse spectra of no-interface (black line), single-interface (red line), and double-interface (blue line) ZnO microwire UV photodetectors on a log scale.

The normalized photocurrent-to-dark current ratio (NPDR), defined as the ratio of responsivity to dark current, is an important parameter to evaluate the weak signal detection ability of a photodetector.[51] The *I*–*V* characteristic curves (Fig. 3) and the photoresponse spectra (Fig. 4) show that although the microwire–microwire interfaces can slightly reduce the UV responsivity of the device, their reduction in dark current is more obvious. Therefore, the NPDR of double-interface ZnO microwire UV photodetector reaches 2.3×10^{10} W^{-1}, which is nearly 5 orders of magnitude higher than that of no-interface device.

The time-dependent photoresponse properties of the ZnO microwire UV photodetectors were investigated at 45 V bias by periodically switching on and off 365 nm illumination with a power intensity of 0.8 mW/cm^2. Figure 5(a) presents the *I*–*t* curves of no-interface, single-interface, and double-interface ZnO microwire UV photodetectors. Obviously, all three devices exhibit reproducible and stable photoresponse to peri-

odic UV illumination. It should be noticeable that the current of the double-interface device rapidly decreases by more than 4 orders of magnitude after switching off the illumination, reaching the level of the initial dark current. According to the single normalized on/off cycle of the time response curves (Fig. 5(b)), the decay times (the time required for the photocurrent to decrease from 90% to 10% of its maximum value) of no-interface, single-interface, and double-interface ZnO microwire devices could be estimated to be ~ 95 s, ~ 3 s and ~ 0.65 s, respectively. Interestingly, the introduction of the microwire–microwire interfaces significantly improves the response speed.

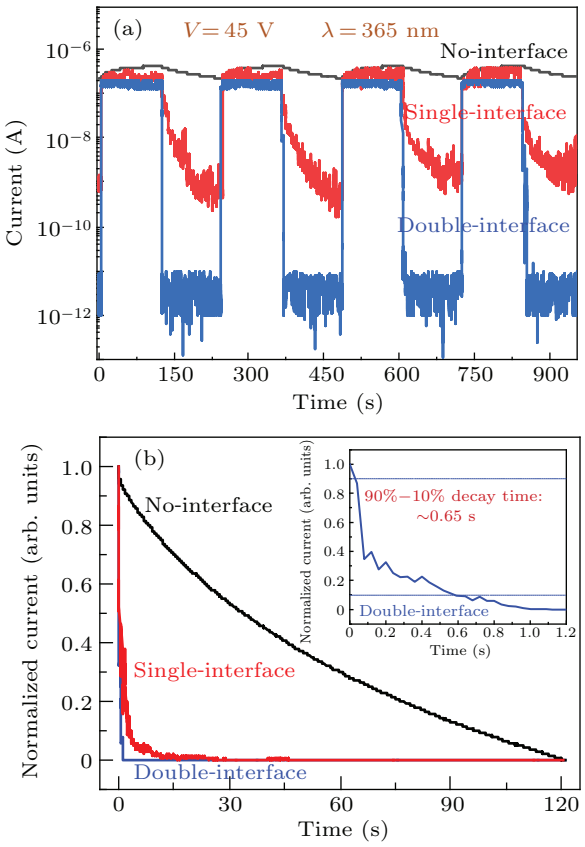


Fig. 5. (a) The *I*–*t* curves of no-interface (black line), single-interface (red line), and double-interface (blue line) ZnO microwire UV photodetectors on a log scale under 365 nm light illumination at a bias voltage of 45 V. (b) Transient photocurrents of three devices normalized at their peak value.

To better understand the mechanism of the photodetection performance enhancement, the energy band diagram of the ZnO microwire photodetector with double wire–wire interfaces is illustrated in Fig. 6. In the dark condition, the potential barriers formed at the wire–wire interfaces could inhibit the transport of free carriers between ZnO microwires, resulting in a lower dark current (Fig. 6(a)). Under illumination, photogenerated electron–hole pairs are generated in ZnO microwires and subsequently separated and drifted by the applied electric field. Meanwhile, when the photogenerated holes drift to the wire–wire interfaces, they would be trapped by the interface states, thereby reducing the barrier height (Fig. 6(b)). And the decreased wire–wire barrier under UV light illumination produces a large photocurrent. After switching off the illumination, the trapped holes at the wire–wire interfaces would be dispersed rapidly and the barrier height would be recovered to its initial dark state value, leading to a small dark current and a relatively fast response speed.

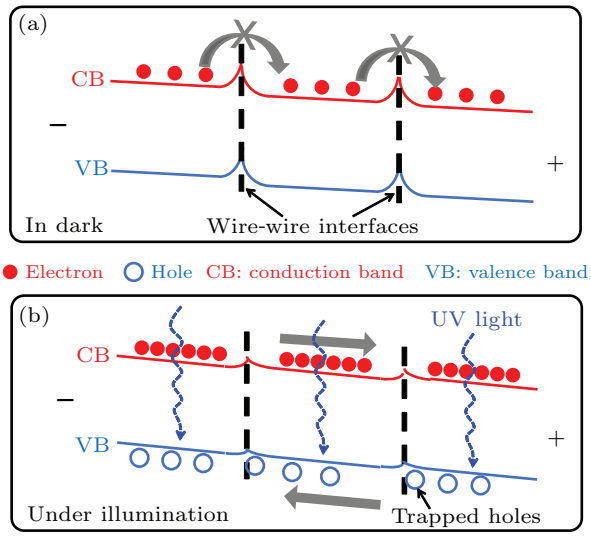


Fig. 6. The energy band diagram of the double-interface ZnO microwire photodetector (a) in the dark and (b) under UV light illumination.

4. Conclusion

In summary, highly crystallized ZnO microwires are synthesized by a simple one-step CVD method. The UV photodetector is built from three cross-intersecting ZnO microwires on a glass substrate with double microwire–microwire homo-interfaces. The dark current of this double-interface device is only about 3.52×10^{-12} A at 45 V, which is almost 5 orders of magnitude lower than that of no-interface reference device. Moreover, compared with no-interface reference device, the NPDR of the double-interface ZnO microwire UV photodetector is improved by nearly 5 orders of magnitude, reaching about 2.3×10^{10} W^{-1}. Meanwhile, the 90% to 10% decay time of this double-interface device is only about 0.65 s. Our analysis shows that the giant performance enhancement for the double-interface device originates from the mechanical contact homo-interfaces. The existence of potential barriers at the interfaces leads to highly suppressed dark current of the device, and it also produces a fast and sensitive photoelectric response due to the barrier height modulation. The results in this work not only provide the insights into the regulation of efficient carrier transport in photodetectors, but also open up tremendous opportunities for the design and development of high-performance optoelectronic devices.

Acknowledgements

Project supported by the National Natural Science Foundation of China (Grant Nos. 62074148, 61875194, 11727902,

12074372, 11774341, 11974344, 61975204, and 11804335), the National Ten Thousand Talent Program for Young Top-notch Talents, the Key Research and Development Program of Changchun City (Grant No. 21ZY05), the 100 Talents Program of the Chinese Academy of Sciences, Youth Innovation Promotion Association, CAS (Grant No. 2020225), Jilin Province Science Fund (Grant No. 20210101145JC), and XuGuang Talents Plan of CIOMP.

References

[1] Liu K, Sakurai M and Aono M 2010 *Sensors (Basel)* **10** 8604

[2] Chen H, Liu K, Hu L, Al-Ghamdi A A and Fang X 2015 *Mater. Today* **18** 493

[3] Higashiwaki M, Kaplar R, Pernot J and Zhao H 2021 *Appl. Phys. Lett.* **118** 200401

[4] Chen X, Wang L, Liu K, Zhang Z, Li B, Wu J, Wang J, Ni Y and Shen D 2020 *J. Mater. Chem. C* **8** 1089

[5] Zhu Y, Liu K, Wang X, Yang J, Chen X, Xie X, Li B and Shen D 2017 *J. Mater. Chem. C* **5** 7598

[6] Ma H, Liu K, Cheng Z, Zheng Z, Liu Y, Zhang P, Chen X, Liu D, Liu L and Shen D 2021 *Chin. Phys. B* **30** 087303

[7] Zhou C, Ai Q, Chen X, Gao X, Liu K and Shen D 2019 *Chin. Phys. B* **28** 048503

[8] Chen Y, Su L, Jiang M and Fang X 2022 *J. Mater. Sci. Technol.* **105** 259

[9] Yang J, Liu K, Chen X and Shen D 2022 *Prog. Quant. Electron.* **83** 100397

[10] Mauthe S, Baumgartner Y, Sousa M, Ding Q, Rossell M D, Schenk A, Czornomaz L and Moselund K E 2020 *Nat. Commun.* **11** 4565

[11] Zhao X, Li Q, Xu L, Zhang Z, Kang Z, Liao Q and Zhang Y 2021 *Adv. Funct. Mater.* **32** 2106887

[12] Shen G and Chen D 2010 *Recent Pat. Nanotech.* **4** 20

[13] Yan R, Gargas D and Yang P 2009 *Nat. Photonics* **3** 569

[14] Tian W, Lu H and Li L 2015 *Nano Res.* **8** 382

[15] Jia C, Lin Z, Huang Y and Duan X 2019 *Chem. Rev.* **119** 9074

[16] Kumar D, Bai R, Chaudhary S and Pandya D 2017 *Mater. Today Energy* **6** 105

[17] Tien L C, Shih Y, Chen C, Huang Y and Chen R 2021 *J. Alloy. Compd.* **876** 160195

[18] Jiang W, Zheng T, Wu B, Jiao H, Wang X, Chen Y, Zhang X, Peng M, Wang H, Lin T, Shen H, Ge J, Hu W, Xu X, Meng X, Chu J and Wang J 2020 *Light Sci. Appl.* **9** 160

[19] Zhang X, Liu B, Liu Q, Yang W, Xiong C, Li J and Jiang X 2017 *ACS Appl. Mater. Inter.* **9** 2669

[20] Gonzalez-Posada F, Songmuang R, Den Hertog M and Monroy E 2012 *Nano Lett.* **12** 172

[21] Delaunay P, Nguyen B M, Hofman D and Razeghi M 2007 *Appl. Phys. Lett.* **91** 231106

[22] Wang X, Zhang Y, Chen X, He M, Liu C, Yin Y, Zou X and Li S 2014 *Nanoscale* **6** 12009

[23] Dai J, Xu C, Xu X, Guo J, Li J, Zhu G and Lin Y 2013 *ACS Appl. Mater. Inter.* **5** 9344

[24] Liu K, Sakurai M, Aono M and Shen D 2015 *Adv. Funct. Mater.* **25** 3157

[25] Liu X, Gu L, Zhang Q, Wu J, Long Y and Fan Z 2014 *Nat. Commun.* **5** 4007

[26] Soci C, Zhang A, Xiang B, Dayeh S A, Dpr Aplin, Park J, Bao X Y, Lo Y H and Wang D 2007 *Nano Lett.* **7** 1003

[27] Shi L, Wang F, Li B, Chen X, Yao B, Zhao D and Shen D 2014 *J. Mater. Chem. C* **2** 5005

[28] Shi H, Cheng B, Cai Q, Su X, Xiao Y and Lei S 2016 *J. Mater. Chem. C* **4** 8399

[29] Fu X W, Liao Z M, Xu J, Wu X S, Guo W and Yu D P 2013 *Nanoscale* **5** 916

[30] Das S N, Moon K, Kar J P, Choi J, Xiong J, Lee T and Myoung J 2010 *Appl. Phys. Lett.* **97** 022103

[31] Chai G Y, Chow L, Lupan O, Rusu E, Stratan G I, Heinrich H, Ursaki V V and Tiginyanu I M 2011 *Solid State Sci.* **13** 1205

[32] Li H, Zhang X, Liu N, Ding L, Tao J, Wang S, Su J, Li L and Gao Y 2015 *Opt. Express* **23** 21204

[33] Ghamgosar P, Rigoni F, You S, Dobryden I, Kohan M G, Pellegrino A L, Concina I, Almqvist N, Malandrino G and Vomiero A 2018 *Nano Energy* **51** 308

[34] Luo Y, Dong Z, Chen Y, Zhang Y, Lu Y, Xia T, Wang L, Li S, Zhang W, Xiang W, Shan C and Guo H 2019 *Opt. Mater. Express* **9** 2775

[35] Zhu X, Lin F, Chen X, Zhang Z, Chen X, Wang D, Tang J, Fang X, Fang D, Liao L and Wei Z 2020 *Nanotechnology* **31** 444001

[36] Gou G, Dai G, Qian C, Liu Y, Fu Y, Tian Z, He Y, Kong L, Yang J, Sun J and Gao Y 2016 *Nanoscale* **8** 14580

[37] Li F, Meng Y, Dong R, Yip S, Lan C, Kang X, Wang F, Chan K S and Ho J C 2019 *ACS Nano* **13** 12042

[38] Gou G, Dai G, Wang X, Chen Y, Qian C, Kong L, Sun J and Yang J 2017 *Appl. Phys. A-Mater.* **123** 731

[39] Chen Y, Wang Y, Wang Z, *et al*. 2021 *Nat. Electron.* **4** 357

[40] Wu P, Ye L, Tong L, Wang P, Wang Y, Wang H, Ge H, Wang Z, Gu Y, Zhang K, Yu Y, Peng M, Wang F, Huang M, Zhou P and Hu W 2022 *Light-Sci. Appl.* **11** 6

[41] Ge H, Xie R, Guo J, Li Q, Yu Y, He J, Wang F, Wang P and Hu W 2022 *Acta. Phys. Sin.* **71** 110703 (in Chinese)

[42] Wu Y, Fan R and Yang P 2002 *Nano Lett.* **2** 83

[43] Clark T E, Nimmatoori P, Lew K K, Ling P and Dickey E C 2008 *Nano Lett.* **8** 1246

[44] Tian B, Xie P, Kempa T J, Bell D C and Lieber C M 2009 *Nat. Nanotechnol.* **4** 824

[45] Wang Z 2009 *Mat. Sci. Eng. R.* **64** 33

[46] Zhao B, Wang F, Chen H, Zheng L, Su L, Zhao D and Fang X 2017 *Adv. Funct. Mater.* **27** 1700264

[47] Qi J, Hu X, Wang Z, Li X, Liu W and Zhang Y 2014 *Nanoscale* **6** 6025

[48] Ai Q, Liu K, Ma H, Yang J, Chen X, Li B and Shen D 2018 *J. Mater. Chem. C* **6** 11368

[49] Harada Y, Tanahashi I and Ohno N 2009 *J. Lumin.* **129** 1759

[50] Lu Y, Zhang Z, Yang X, He G, Lin C, Chen X, Zang J, Zhao W, Chen Y, Zhang L, Li Y and Shan C 2022 *Nano Res.* **15** 7631

[51] Wang X, Cheng Z, Xu K, Tsang H K and Xu J 2013 *Nat. Photonics.* **7** 888